Vol. 81 No. 2 pp. 297–311 ACTA GEOLOGICA SINICA April 2007

Rock Deformation, Component Migration and $^{18}O/^{16}O$ Variations during Mylonitization in the Southern Tan-Lu Fault Belt

YANG Xiaoyong[1,2], LIU Deliang[1], FENG Min[1], YU Qingni[1] and WANG Kuiren[1]
1 *CAS Key Laboratory of Crust-Mantle Materials and Environments, School of Earth and Space Sciences, University of Science and Technology of China, Hefei, Anhui 230026*
2 *CAS Key Laboratory of Isotope Geochronology and Geochemistry, Guangzhou Institute of Geochemistry, Guangzhou, Guangdong 510640*

Abstract: This paper discusses the relationship between the volume loss, fluid flow and component variations in the ductile shear zone of the southern Tan-Lu fault belt. The results show that there is a large amount of fluids flowing through the shear zone during mylonitization, accompanied with the loss of volume of rocks and variations of elements and oxygen isotopes. The calculated temperature for mylonitization in different mylonites ranges from 446 to 484°C, corresponding to that of 475 to 500°C for the wall rocks. The condition of differential stress during mylonization has been obtained between 99 and 210 MPa, whereas the differential stress in the wall rock gneiss is 70–78 MPa. The mylonites are enriched by factors of 1.32–1.87 in elements such as TiO_2, P_2O_5, MnO, Y, Zr and V and depleted in SiO_2, Na_2O, K_2O, Al_2O_3, Sr, Rb and light REEs compared to their protolith gneiss. The immobile element enrichments are attributed to enrichments in residual phases such as ilmentite, zircon, apatite and epidote in mylonites and are interpreted as due to volume losses from 15% to 60% in the ductile shear zone. The largest amount of SiO_2 loss is 35.76 g/100 g in the ductile shear zone, which shows the fluid infiltration. Modeling calculated results of the fluid/rock ratio for the ductile shear zone range from 196 to 1192 by assuming different degrees of fluid saturation. Oxygen isotope changes of quartz and feldspar and the calculated fluid are corresponding to the variations of differential flow stress in the ductile shear zone. With increasing differential flow stress, the mylonites show a slight decrease of $\delta^{18}O$ in quartz, K-feldspar and fluid.

Key words: mylonitization, ductile shear zone, component migration, oxygen isotopes, southern Tan-Lu fault belt

1 Introduction

Because mylonites record some special phenomena in the geological process of crustal deformation (Tullis et al., 1982), geologists all over the world have paid great attention to them from various aspects. In the recent two decades, many researchers have contributed to the study of thermal fluids which play major roles in the process of metamorphism, especially in that of metamorphism-deformation in the ductile shear zone (Engelder, 1984; Ferry, 1986; Wood, 1986; O'hara et al., 1988, 1994; Glazner et al., 1991; Newman et al., 1993; Julie et al., 1999; Jefferies et al., 2006). Each of them has studied the effect of regional or partial fluids to the shearing deformation and metamorphism from different aspects. They revealed the close relationship between the fluids and ductile deformation supported by structural, petrologic and geochemical lines of evidence (e.g. Kerrich, 1986; Segall and Simpson, 1986; Burkhard et al., 1988; MaCaig, 1988; O'hara et al., 1989; Gibson, 1990; Kronenberg et al., 1990; Glazner and Barttey, 1991; Tobisch et al., 1991; Pennacchioni et al., 1996, 1997; Yang et al., 1998a; Kisters et al., 2000). Evidences for substantial fluid migration through active shear zones in middle-crustal environments are commonly indicated by the change in bulk rock and mineral composition of shear zone rocks relative to their protoliths (Streit and Cox, 1998; Bauer et al., 2000). Mattey et al. (1994) studied the isotopic constrains on fluid infiltration and deep deformation processes from eclogite facies shear zones in Norway. The eclogite-facies shear zones have been identified, representing deep crustal reflectors in portions of the crust that experienced high-pressure conditions but escaped thermal reactivation (e.g., Fountain et al., 1994; Torgeir et al., 2005). The dating of mylonites with different isotopic systems has been undertaken, which shows prosperous results with special dealing to the tectonic rocks (e.g., Müller et al., 2000;

* Corresponding author. E-mail: xyyang@ustc.edu.cn.

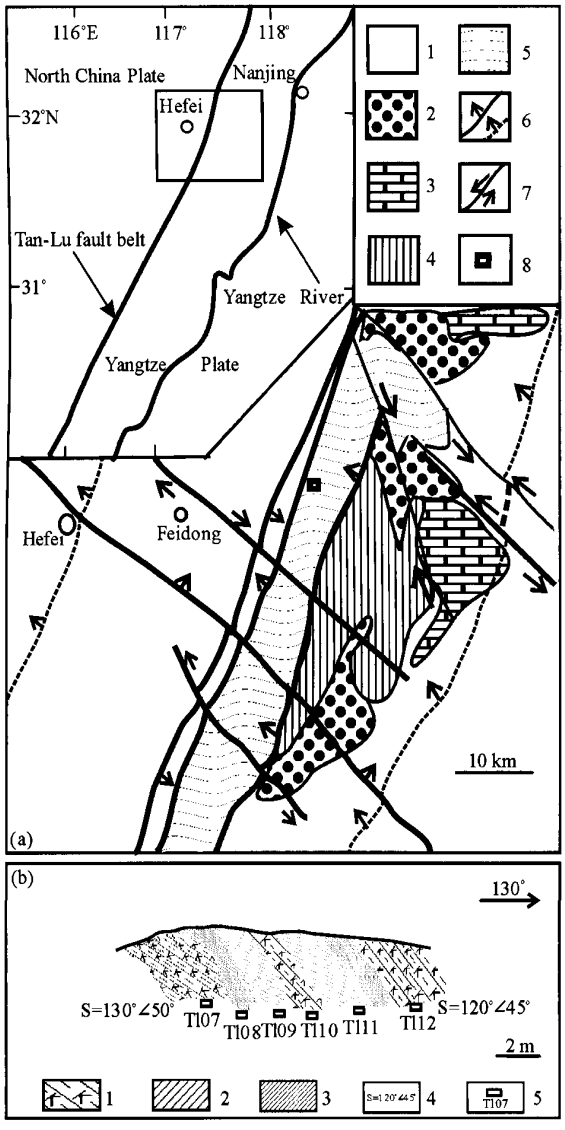

Fig. 1. Geological map and profile of the ductile shear zone in the south Tan-Lu fault belt.

(a) Geological map (1. Lower Cretaceous Series-Tertiary System; 2. Upper Cretaceous Series; 3.Cambrian-Silurian Systems; 4. Sinian System; 5. Lower Proterozoic-Lower Archean erathem; 6. reversed fault; 7. strike fault; 8. locality of the studied ductile shear zone).

(b) Geological sections and sampling localities in the ductile shear zone (1. potassic feldspar gneiss; 2. protomylonite; 3. mylonite; 4. cleavage of deformed rocks; 5. sampling locality).

Wang and Lu, 2000; Mulch et al., 2002; Phillips et al., 2004; Zhu et al, 2004).

Owing to the above investigations of ductile shear zones and mylonites, Samantaa et al. (2002) developed different types of pull-apart microstructures in mylonites by experimental investigation; Schenk et al. (2005) studied the effect of water on recrystallization behavior and grain boundary morphology in calcite through observations of natural marble mylonites; Dong et al. (2006) reviewed the advances in studies of deformation mechanisms and rheology of rocks of large-scale strike slip faults and indentation-extrusion tectonics. Arjan et al. (2002) studied the role of melt-rock reaction in mantle shear zone formation in Greece peridotite massif. These studies present broad knowledge for ductile shear zones and mylonites.

The area for this study is in the joint part of the Tan-Lu fault belt with the East Qinling-Dabie orogenic belt in the east part of China (Mattauer et al., 1985), where the compression and nappe structures, elongation by stress and shearing system are well-developed and different layers of rocks from the surface of the crust to the upper mantle have good outcrops, which have recorded the history of the geology and evolution of the North China plate and South China plate with multiple splitting, matching and sliding (Xu et al., 1987; Yang et al., 1998b; 2001). Therefore, this area is excellent for understanding the geological and geochemical effects induced by the collision of the North China and South China plates. In this study we chose one ductile shear zone for systematic sampling and analysis of the chemical and isotope compositions of mylonites and wall rock gneiss in order to characterize the relationship between deformation and fluid-rock interaction during mylonitization.

2 Geological Setting and Sampling

There are a series of ductile shear zones also with NE or NNE directions developed in the slide formation of the major fault belt, which have been studied by many Chinese scholars in various aspects: Lu et al. (1983) once studied the changing stress field in the middle segment of this fault belt; Lin et al. (1998) found that the Tan-Lu fault belt in Shandong Province north to this studied region has some characteristics of Quaternary activity. The southern part of the Tan-Lu fault belt is of special importance for understanding the geological event of the Dabie and Sulu terranes since the Triassic, for it is this effect that cut through the two terranes since the Cretaceous and made them some 550 km apart from each other since then (Fig. 1a). Lin et al. (2005) presented the Triassic polyphase deformation in the Feidong-Zhangbaling massif eastern of the Tan-Lu fault belt related to its place in the collision between the North China and South China blocks. Zhu et al. (2004) obtained the $^{40}Ar/^{39}Ar$ ages of mylonite whole-rock and muscovite from the later Tan-Lu ductile shear zone, suggesting a sinistral strike-slip cooling event at 128 Ma. Up to now, many studies were focused on the field geology, features of rock deformation, regional structural strain field and tectonic evolution, and not concerned about the chemical changes in the formation of mylonites of the ductile shear zones belonging to the Tan-Lu fault system. The ductile shear zones are important for understanding the

Table 1 Stratigraphic formation of gneiss in the Tan-Lu fault

Age	Group	Formation	Characteristics of rocks
Paleoproterozoic (1900 Ma)	Feidong	Qiaotouji	>500 m, mainly composed of amphbolite schist, biotite schist and amphibole-biotite-plagioclase gneiss
		Shuangshan	>274 m, mainly composed of phosphatic carbonate formation with minor plagioclase amphibolite and tremolite
Neoarchean (2500 Ma)	Kanji	Dahengshan	>1278 m, mainly composed of amphibolite with multiple layers
		Fuchashan	>2393 m, mainly composed of biotite-plagioclase gneiss with inter-beds of plagioclase amphibolite and acid volcanic rocks; ductile shear zones and various mylonites are well-developed in this group

Table 2 Minerals assemblages of the rocks in Tan-Lu fault belt

	Sample No.	TL07	TL08	TL09	TL10	TL11	TL12
	Rock types	gn	pr	my	gn	my	gn
Minerals	Quartz	30	40	45	30	35	25
	K-feldspar	40	32	15	45	15	40
	Plagioclase	20	12	10	15	20	20
	Muscovite	2	5	10	2	15	3
	Biotite	3	2	5	3	5	4
	Chlorite	-	3	5	-	2	-
	Epidote/Zoisite	-	+	6	-	4	-
	Zircon	+	1	1	+	1	+
	Apatite	1	1	1	1	1	1
	Calcite	1	1	+	1	+	1
	Opaque minerals	1	1	2	1	3	1

Note:. denotes the minerals with contents less than 1%; - denotes the minerals unfound in the thin section; gn-gneiss; pr-protomylonite; my-mylonite

evolution history of the Tan-Lu fault system as well as the evolution of the Dabie and Sulu terranes since the Cretaceous., for they are the main part of the Tan-Lu fault system which was developed in the middle to lower crust, whose tectonic rocks — a series of mylonites in the shear zones can present lots of information of the middle and lower crust. This study pays attention to the mylonites in the ductile shear zones, especially those concerning the chemical changes as well as the characteristics of deformation during the formation and evolution of the ductile shear zones. The studied area chosen is in Feidong and Chaoxian counties of Anhui Province, East China, where many well-developed ductile shear zones can be found in the fault belt. According to the regional geological information, the outcropping rocks in the ductile shear zone belong to the Kanji Group and Feidong Group, whose stratigraphic characteristics are summarized in Table 1. From the field observation, it can be found that the angles of strike of the ductile shear zone are between 10° and 30°, being about parallel to each other, and in the same direction with the elongation of the Tan-Lu fault belt. The movement of the Tan-Lu fault belt could have led to the large-scale migration and convergence of fluids toward foreland basins induced during the collisional orogeny of the Yangtze and North China continental blocks, as vital importance for the formation of the metallogenic belt nearby (Hou et al., 2004).

The ductile shear zone is located in the Kanji Formation as shown in Table 1 and the wall rocks of the ductile shear zone are K-feldspar gneiss, biotite two feldspar gneiss. The deformed rocks in the ductile shear zone are felsic mylonite, streak and augen ultra-mylonites according to their intensity of deformation, respectively. The contact boundaries between the edge of the shear zone and wall rocks are clear and the ductile shear zones are developed symmetrically, i.e., the mylonitic rocks are strongly deformed rocks in the center and gradually change into weakly deformed ones on the edges of the ductile shear zone. The width of the ductile shear zones is not large (often less than 30 m).

We collected 6 samples (3 mylonite and 3 wall rock—gneiss) in one complete ductile shear zone for this study (profile section Fig. 1b).

3 Mineralogy and Petrology

3.1 Mineral assemblage

Compared with the wall rocks of gneiss, the mylonites in the ductile shear zone have similar rock-forming minerals, but the percentages of the minerals in the two are quite different. The mylonites display conspicuous concentration of accessory phrases such as apatite, zircon, ilmentite and epidote. Table 2 lists the percentages of major rock-forming minerals and minor minerals both in the wall rocks and in the tectonic rocks from the above ductile shear zone. Figure 2 shows the mineral component variations in the ductile shear zone, from which it can be seen that with the increase of deformed intensity in the ductile shear zone, i.e., from the wall rocks to the tectonic rocks, the content of quartz gradually increases, while that of feldspar decreases, accompanied with muscovite and epidote increasing, chlorite to some extent increasing, and biotite decreasing. The evidence is represented by the grain-size reduction of feldspar and biotite, thus biotite cannot be seen in the

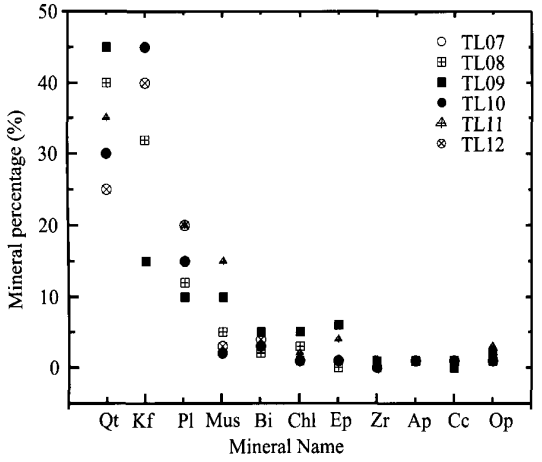

Fig. 2. Mineral assemblages showing different mineral component variations in the ductile shear zone.

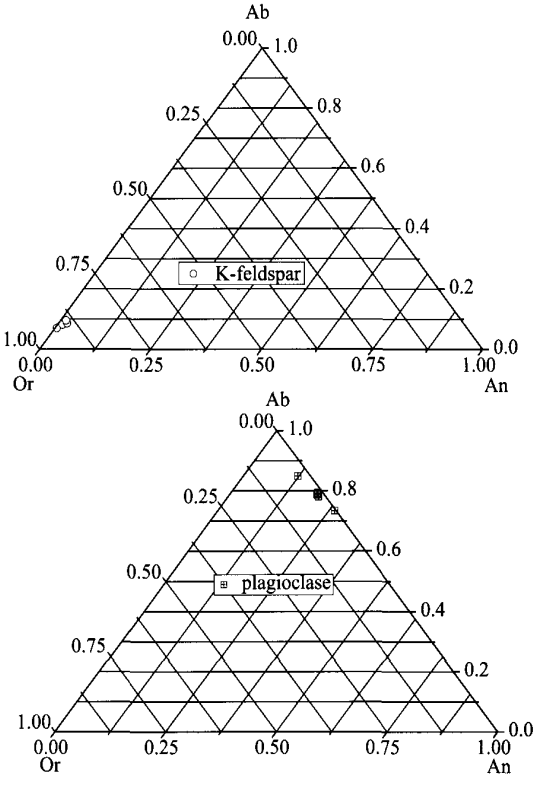

Fig. 3. The ternary diagram showing the compositional distributions of feldspars from the rocks in ductile shear zone of the south Tan-Lu fault belt.

models, and epidote is often seen in aggregates of crystals.

3.2 Feldspar compositions and temperature condition

Chemical analysis on single feldspar was carried out on the Jeol JXA-50A electron microprobe equipped with 5WDS spectrometers at 15kV, 15nA, 10nA, 100 cps and a CAMECA SX50 with the link EDS system controlled by software. The measurement was taken in the laboratory of the Institute of Uranium Geology, Beijing. The results are listed in Table 3.

Table 3 The chemical compositions of feldspars from the mylonites and their wall-rocks in the ductile shear zone, south Tan-Lu fault belt

Mineral	Sample No.	SiO_2	TiO_2	Al_2O_3	FeO	MnO	MgO	CaO	Na_2O	K_2O	Total	Or	Ab	An	T(°C)
K-feldspar	TL07	64.17	0.15	18.26	0.12	–	0.02	–	1.10	16.11	99.93	90.64	9.36	–	495
	TL08	63.36	0.11	18.08	0.03	0.01	–	0.08	0.79	15.99	98.45	92.60	6.99	0.41	446
	TL09	64.37	0.37	18.07	0.07	–	–	0.04	0.74	16.58	100.24	93.46	6.33	–	454
	TL10	64.49	0.42	17.99	–	0.06	–	0.25	0.97	16.52	100.70	90.73	8.14	1.13	475
	TL11	64.64	0.40	17.17	0.04	–	–	0.42	1.03	16.38	100.08	89.50	8.59	1.91	484
	TL12	64.66	0.35	17.35	0.02	0.01	–	0.26	1.15	16.27	100.07	89.26	9.55	1.19	500
Plagioclase	TL07	63.82	–	22.29	0.10	–	0.07	4.00	8.96	0.18	99.42	1.07	79.37	19.56	
	TL08	65.08	0.03	20.82	0.03	0.05	–	2.44	9.38	0.48	98.31	2.84	84.95	12.21	
	TL09	62.28	0.08	23.95	0.14	0.04	–	5.26	8.13	0.05	99.93	0.30	73.44	26.26	
	TL10	64.53	0.02	21.88	0.09	0.04	–	3.95	8.88	0.20	99.59	1.15	79.36	19.49	
	TL11	65.28	–	21.60	0.21	0.05	–	4.06	8.99	0.28	100.47	1.59	78.77	19.64	
	TL12	65.27	–	21.94	0.04	–	–	4.28	9.13	0.28	100.94	1.59	78.14	20.27	

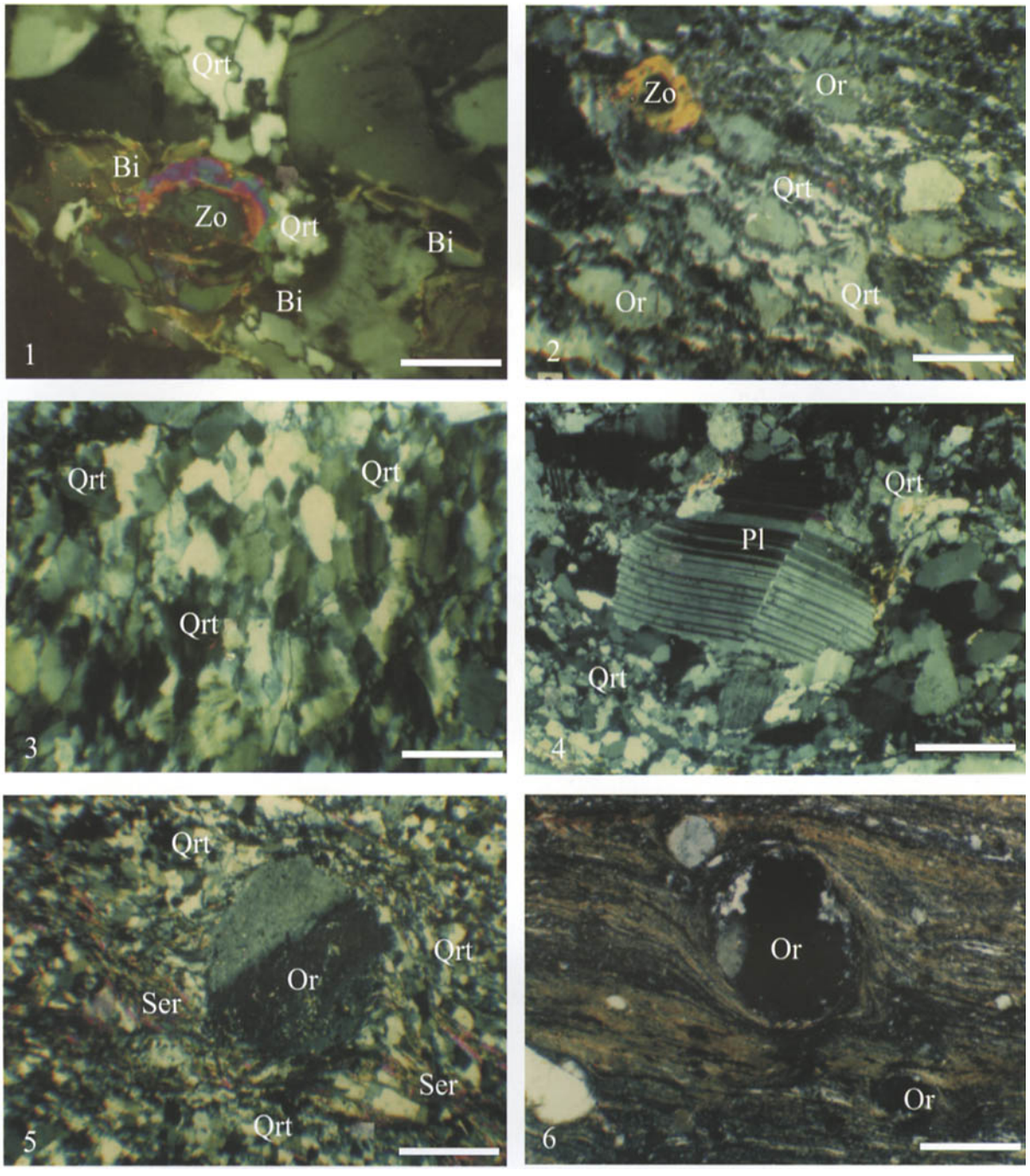

Fig. 4. Explanations of micro-structure characteristics of wall rocks and mylonites in the south Tan-Lu fault belt.

(1) Zoisite (Zo) occurs as xenomorphic to idiomorphic euhedral crystals, replacing biotite (Bi) in protomylonites (crossed light, scale bar 0.50 mm, TL07); (2) quartz (Q), orthoclase (Or), sericite, epidote and chlorite in various grain sizes occur in parallel bands (crossed light, scale bar 0.50 mm, TL08); (3) quartz (Q) of a plastic deformation band with strong undulatory extinction and grain-size reduction (crossed light, scale bar 0.35 mm, TL09); (4) a kink in feldspar twins (Pl) indicating on-going grain-size reduction (crossed light; scale bar 0.35 mm, TL09); (5) typical microscopic appearance of ultramylonite with augen structure of orthoclase (Or). The drag mark is composed of fine-grained sericite (Ser) and quartz (Q) (crossed light; scale bar 0.35 mm, TL11); (6) typical microscopic appearance of ultramylonite with complex σ-δ feldspar grain structure, both σ and δ tails of orthoclase (Or) step up to the left and become parallel to foliation, consistent with the sinistral shear sense (crossed light; scale bar 0.35 mm, TL11).

The feldspars can be classified into three types, i.e., potassium feldspar (K-feldspar), albite and plagioclase. The ternary diagram of feldspars (Fig. 3) can be drawn from the data of Table 3, and it can be seen that the components in K-feldspar do not contain a single plagioclase molecule (in the limit of the measurement) but with high contents of K-feldspar molecules (Or=87.26%–93.46%), belonging to the pure K-feldspar. The plagioclase

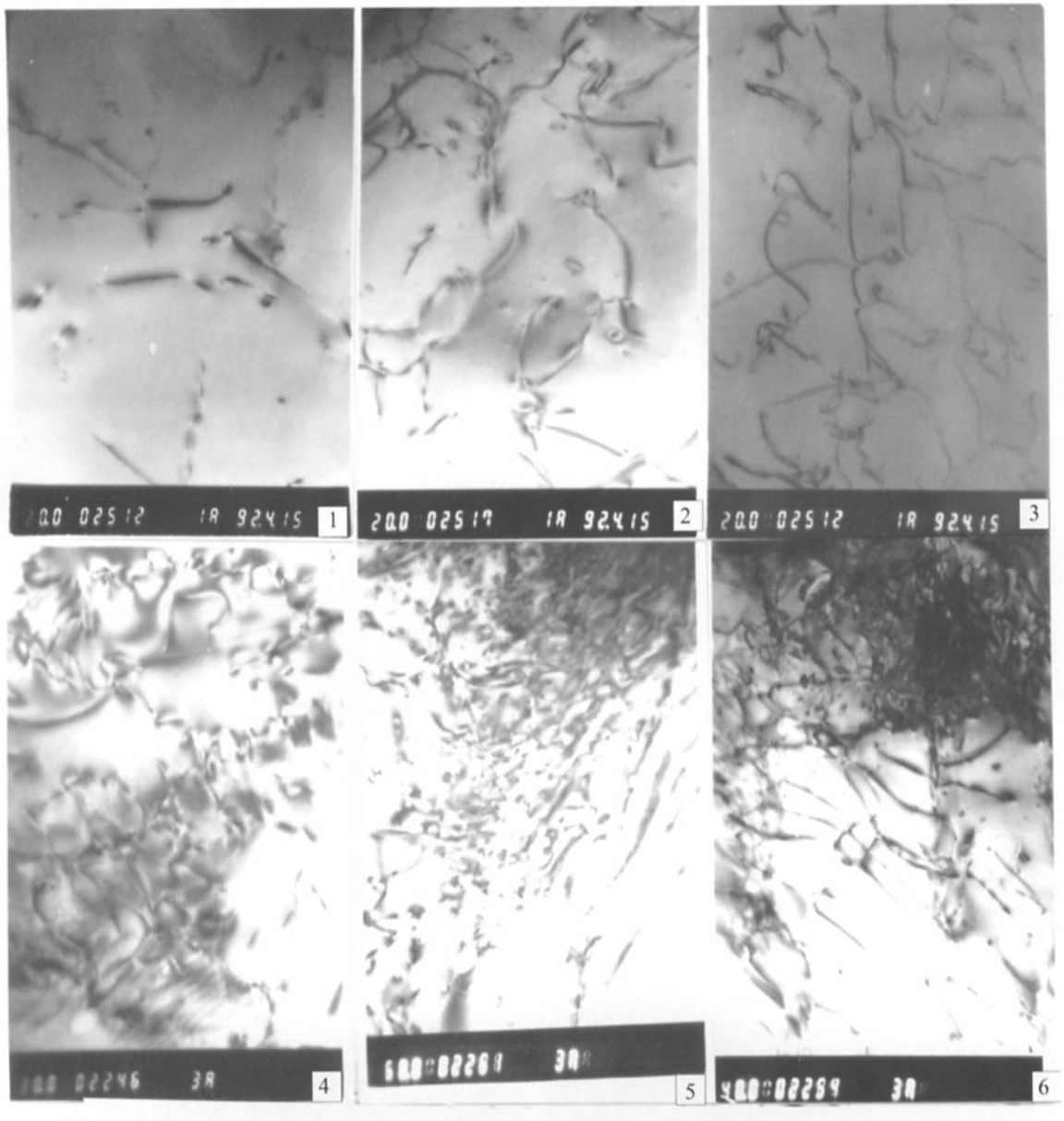

Fig. 5. Ultra-microstructural features of mylonitic rocks obtained by the TEM.
(1) The dislocation net consisting of short and curved dislocations in quartz (′20000, TL08); (2) the high density of dislocations which forms winds in quartz (′40000, TL08); (3) dislocation net consisting of long and straight dislocations in quartz (′30000, TL09); (4) dislocations with dislocation boundaries and sub-boundaries (′30000, TL09); (5) dislocations with triple nodes, small dislocation loops (′20000, TL11); (6) dislocations with dislocation boundaries and sub-boundaries (′4000, TL11).

belongs to the acid oligoclase generally with less than 20% of An content (maximum 26.26%), which manifests that the original rocks belong to acid rocks. The compositions of feldspars have distinct regional characteristics, i.e., they have high contents of Or molecules and plagioclase has high contents of albite molecules. Figure 3 is a ternary diagram showing the compositional distributions of feldspars in the ductile shear zone.

By using the method of Whitney and Stomer (1977), the calculated temperatures for each pair minerals are also listed in Table 3. The mylonites have their forming temperatures of 446–484°C corresponding to the wall rocks of 475–500°C.

Microscopic observations reveal that the mineral assemblage in the tectonic and wall rocks is quartz + plagioclase + K-feldspar + biotite + muscovite + chlorite (epidote) ± apatite ± titanite ± opaque minerals. According to this assemblage, the temperature and pressure of the deformation and metamorphism can be estimated as 450–600°C and 4×10^9 Pa, respectively, based on the general

Table 4 Differential stress ($\sigma_1-\sigma_3$) in the ductile shear zone of the south Tan-Lu fault belt

Sample No.	Dislocation density (10^8/cm^2)	$\sigma_1-\sigma_3$ (MPa)[1)]	$\sigma_1-\sigma_3$ (MPa) [2)]	$\sigma_1-\sigma_3$ (MPa)[3)]	$\sigma_1-\sigma_3$ (MPa) (Average)
TL07	3.31	70.9	72.1	68.9	70.6
TL08	5.52	100.4	102.3	96.5	99.7
TL09	18.11	206.6	210.5	211.4	209.5
TL10	3.80	78.2	79.8	75.4	77.8
TL11	7.20	119.0	122.0	115.0	118.7
TL12	3.51	73.9	72.3	71.6	72.6

Notes: For the superscripts, [1)] is after Twiss (1986); [2)] and [3)] after Mercier et al. (1977) under dry and wet conditions, repectively.

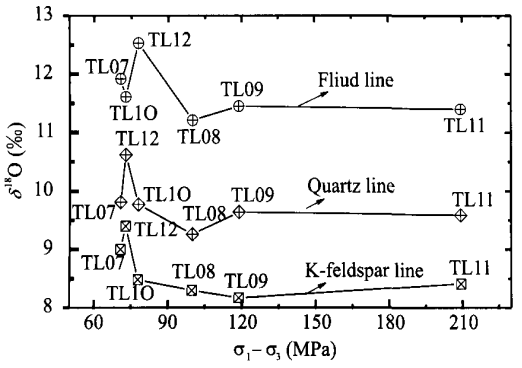

Fig. 6. Variation of the differential flow stress versus oxygen isotopes of the various samples in the ductile shear zone.

mineral stable lines of Mueller and Saxena (1977), which is accordant with the above calculation by means of the two feldspars.

4 Microstructures and Evaluation of Differential Flow Stress during Mylonitization

4.1 Characteristics of microstructures

The characteristics of mylonites show feldspar grains with kinking and twinning, those of biotites show a preferred orientation parallel and sub-parallel to the foliation. Recrystallization, bending, kinking and undulose extinction are common. Quartz occurs as large recrystallized grains located in ribbon- shaped regions. All of these microstructural features in deformed grains in the foliated granitoids indicate subsolidus deformation (Paterson and Vernon, 1995). The structures of these types of mylonites consist of parallel banding and streak structures, complex σ-δ feldspar grain structure, S-C micro -foliation, and the characteristics of kink in feldspar twins and quartz plastic deformation. There is also presentation of a large mount of recystallization and subgrain sizes in deformed quartz in mylonites, which shows relatively strong deformation during mylonization in this area (Mercier et al., 1977; Twiss, 1977).

Figure 4 shows the characteristics of the microstructures of the wall rocks and mylonites in the south Tan-Lu fault belt.

4.2 TEM observation

Optical thin sections (both sides polished) were used for detailed TEM observation. On the basis of the above microscopic observation, we selected the typical structures in the slices for the TEM observation, which recorded the most important ductile deformed history in this region. Firstly, the selected areas from thin sections were ion thinned to electron transparency using Ar^+ at 5 kV. The observation was carried out with an H-800 type TEM made in Japan, with the experimental condition of an accelerating voltage of 200 kV and equipped with a two-axis goniometer. Representative areas were photographed at magnifications of 10000 to 40000 times. Diffraction conditions were adjusted by tilting some specimens to ensure optimum contrast of images. With this equipment, the characteristics of the dislocation in quartz were studied and the plastic deformation of the mylonites discussed. Typically, very high density of dislocation was observed on the deformed quartz, which further confirms the plastic deformation of the mylonites. The most common image is that of high density of dislocation in deformed quartz micro -crystals, such as dislocations with triple nodes, small dislocation loops and dislocation boundaries and sub-boundaries. The typical TEM images and their explanations in details were presented in Fig. 5.

4.3 Differential flow stress

Qualitative information about deformation conditions can often be inferred from general investigations of the subgrain size, micro- or ultral-micro-structures. There are numerous TEM studies on ultra-micro-structures of dislocations (e.g., White et al., 1971; Liddle et al., 1976). Twiss (1986) has established experimentally the relationship between the density of dislocations of deformed quartz and recrystallized grain size. Other studies about paleostress evaluation have been done to the deformation of some mylonites (Christie and Ord, 1980; Etheridge and Wilkie, 1981; Hacher et al., 1992). Although the condition of dislocations with recovery arrangement can interfere with the results of evaluation of paleostress

Table 5 The major element compositions and oxygen isotope of the rocks of the ductile shear zone from the south Tan-Lu fault belt (wt%)

Sample	TL07	TL08	TL09	TL10	TL11	TL12
SiO_2	75.04	73.46	70.16	72.25	69.89	72.66
TiO_2	0.16	0.21	0.40	0.35	0.39	0.15
Al_2O_3	13.26	12.95	14.72	13.07	13.94	13.54
Fe_2O_3	0.22	0.53	0.88	0.61	0.81	0.74
FeO	0.82	1.54	2.03	2.19	2.06	1.26
CaO	1.10	1.19	1.60	1.05	1.48	1.22
MgO	0.09	0.31	0.57	0.29	0.55	0.31
MnO	0.01	0.03	0.04	0.02	0.03	0.03
Na_2O	3.20	3.46	4.00	3.32	3.83	3.28
K_2O	5.40	4.60	3.73	5.20	3.74	5.00
P_2O_5	0.02	0.05	0.01	0.03	0.10	0.05
CO_2	0.09	0.13	0.17	0.14	0.25	0.34
H_2O	0.52	0.68	0.62	0.68	0.70	0.76
L.I.O	0.42	0.40	0.52	0.67	0.67	0.51
Total	100.25	99.54	99.45	99.87	98.44	99.85
ρ	2.590	2.640	2.640	2.600	2.630	2.590
$\delta^{18}O_{(quartz)}$	9.81	9.26	9.59	9.77	9.64	10.62
$\delta^{18}O_{(K\text{-}feldspar)}$	9.00	8.30	8.41	8.48	8.17	9.40
$\delta^{18}O_{(Fluid\text{-}Q)}$	11.91	11.28	11.62	11.84	11.73	12.73
$\delta^{18}O_{(Fluid\text{-}Kf)}$	11.92	11.15	11.27	11.37	11.07	12.32
$\delta^{18}O_{(Fluid)Av.}$	11.92	11.21	11.45	11.61	11.40	12.53

Notes: (1) The elements were analyzed by the Central Lab. of the Institute of East China Metallurgy Co., Hefei, analyst: Liu Wenqi; ρ—density of whole rocks in g/cm^3. (2) Oxygen isotope was analyzed by the Department of Geology, Nanjing University, analyst: Huang Yaosheng; (3) The fluid value of oxygen isotope is calculated by the eqs. $^{18}O_w=18O_Q+2.71-3.57\times10^5\times(1/T^2)[Q-H_2O]$ (Clayton et al., 1972) and $^{18}O_w=18O_{Kf}+3.41-2.91\times10^5\times(1/T^2)[Kf-H_2O]$ (O'Neil and Taylor, 1967) respectively. It can be seen that both the results are similar with the analyzed errors, so we used the average values for discussion.

Table 6 Trace element compositions of rocks from the ductile shear zone of the south Tan-Lu fault belt (μg/g)

Sample	TL07	TL08	TL09	TL10	TL11	TL12
La	24.65	27.25	28.61	29.35	25.40	24.90
Ce	46.13	50.98	51.95	53.13	47.67	48.21
Pr	5.90	6.40	6.88	6.97	6.04	5.90
Nd	25.56	28.22	29.63	30.39	27.53	26.05
Sm	5.78	6.66	6.48	6.69	5.70	5.87
Eu	1.20	1.30	1.40	1.48	1.25	1.20
Gd	7.42	8.19	8.91	9.53	8.35	8.27
Tb	1.34	1.57	1.86	1.90	1.53	1.45
Dy	8.50	9.06	9.59	10.00	9.42	9.33
Ho	1.71	1.78	1.90	1.98	1.65	1.60
Er	5.02	5.97	6.01	6.25	5.50	5.00
Tm	0.59	0.67	0.68	0.69	0.59	0.58
Yb	3.93	4.38	4.50	4.59	3.99	3.87
Lu	0.59	0.63	0.67	0.68	0.59	0.56
Y	8.87	14.06	15.29	8.65	12.75	8.63
Zr	75	121	122	76	120	73
Sr	158	179	181	188	176	165
Pb	45	51	51	54	48	45
Zn	20	25	28	30	24	22
Cu	5	6	8	9	6	5
Ba	1200	1334	1388	1480	1199	1180
Cr	24	25	27	28	23	22
V	16	18	19	13	17	15
Ga	18	18	18	21	18	18
Nb	22	24	26	26	24	22
Ni	4	4	4	5	4	4
Rb	120	138	140	159	129	118

Note: Analyzed by the ICP-Mass Lab. of the Physical-Chemical Analysis Center of the University of Science and Technology of China.

(e.g., Wenk, 1994), fortunately, it seems that there does not exist strong recovery arrangement of dislocations of quartz in this region. So it is very useful to evaluate the paleostress by means of the density of dislocations in quartz and the subgrain size. The parameters and results of the differential flow stress ($\sigma_1-\sigma_3$) of the ductile shear zone by both the density of dislocations in quartz and the subgrain size proposed by Twiss (1986) and Mercier et al. (1977) are listed in Table 4. The condition of the differential flow stress during mylonization has been obtained. The largest differential flow stress of mylonites is 209.5 MPa (with a range of 99.7–209.5 MPa), whereas the flow stress in the wall rock gneiss is 70.6–77.8 MPa.

5 Migration of Chemical Compositions during Mylonitization

5.1 Characteristics of chemical compositions of rocks

In order to calculate using the model, the chemical compositions including both the major and some of minor elements of the bulk rocks were analyzed. And the oxygen isotopes of quartz and K-feldspar are also analyzed for each sample. The results are listed in Tables 5 and 6. In Table 5, the oxygen isotopic data of quartz and K-feldspar are measured with the normal BrF_5 method in the Department of Geosciences, Nanjing University.

5.2 Variations of the oxygen isotopes

The oxygen isotopes of fluids are calculated with the fractionation between quartz and K-feldspar at the temperature of 500°C, using the parameter of Clayton (1972) and O'Neil and Taylor (1967). The calculated oxygen isotopic values of fluids balanced with quartz and K-feldspar are listed in Table 5, from which it can be seen that the values from both quartz and K-feldspar are very close within the analytical errors, which proves that the fluid was once balanced with mineral reaction for the oxygen isotope exchange between quartz and K-feldspar in the ductile shear zone.

Combined with Table 4 and the oxygen isotopic data in

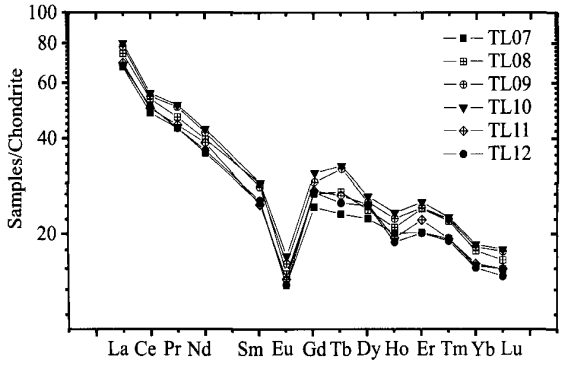

Fig. 7. REE distribution patterns of different samples in the ductile shear zone.

Table 5, we have obtained the plot of Fig. 6, which shows the relationship between the differential flow stress of rocks corresponding to the oxygen isotopic changes of quartz and feldspar and the calculated fluid. From the diagram, we can see that the oxygen isotopic changes correspond to the variations of differential flow stress in the ductile shear zone. With the increasing differential flow stress, the mylonites (samples TL 08, 09, 11) show a slight decrease of $\delta^{18}O$ in quartz, K-feldspar and fluids, with larger fluctuations in the wall rock—gneiss (samples TL 07, 10, 12).

5.3 REE distribution patterns

The REE distribution patterns of the mylonites and gneiss are shown in Fig. 7. From the diagram, it can be seen that all the rocks have a large negative Eu anomaly and almost with the same patterns of REE distributions. Still there are also some distinguished differences between these rocks, such as the concentration of REEs in different rock types.

5.4 Calculation of volume factors in metamorphism-deformation reaction

According to the equation of Gresens (1967), the relationship between the composition and volume in a rock chemical reaction can be obtained by the following equation,

$$\Delta X_n = a \times [F_v \times X_n^B (\rho^A/\rho^B) - X_n^A] \quad (1)$$

where X_n = chemical transfer in grams of component n between the parent rock A and the product rock B; ΔX_n = the gain and loss of component n during the reaction (if the component is in wt%, then the unit is in g); a = mass of parent rock (if a=100, then X_n=g/100 g or wt%); F_v = ratio of the final to the initial volume of rock (V_B/V_A); X_n^B and X_n^A = wt% fraction of chemical component n in rock A and B, respectively; ρ^A and ρ^B = density of rock A and B, respectively.

In equation (1), the key problem for calculation is the determination of volume factor F_v. According to the simple solution and deduction of equation (1) by Grant (1986), a composition to composition diagram can be drawn in the relation of parent rock to daughter rock.

Now take the example in metamorphic reaction pair (TL07→TL08), we used the average contents of gneiss and mylonite of the samples to study the component variations in the chemical reaction A→B. According to the above discussion, the diagram of C_n^A-C_n^B is plotted as Fig. 8a. In the diagram, two linear trends can be identified during the process of metamorphic reaction of gneiss→mylonite: one is with a slope of around 1 ($C_n^A = C_n^B$), the other with a slope of 1.46 (C_n^B=1.46 C_n^A). Of course, one of the above two lines belongs to the real metamorphic reaction during the formation of the ductile shear zone according to Grant (1986). However, which one is suitable for the determination of F_v during the metamorphic reaction? In order to answer this question, we must first check the elements or components coming through or near the two lines. The line with a slope of 1 passes close to or through SiO_2, K_2O, Na_2O, Al_2O_3, Sr, Pb, Rb and some light REEs (La, Ce and Nd); all the elements above the line would then be inferred to have added to the system under isovolumetric conditions; and the other line with a slope of 2.53 passes to or through TiO_2, P_2O_5, MnO, V, Zr, Y and ΣFe_2O_3. If we take the first line as the metamorphic reaction, it will imply that element such as Ti, P, Mn, Zr and Y were added to the system while the relatively soluble elements such as SiO_2 and alkali remained constant. Such a situation is not thought to be realistic, since Ti, P, Mn, Zr and Y are commonly regarded as some of the most insoluble elements (Cann, 1970; Correns, 1978; Herrmann, 1978; Landergren, 1978). For example, the solubility of Ti can only reach 5–50 ppb in natural water (Correns, 1978), whereas SiO_2 and alkalis are some of the most soluble (Cann, 1970; Faure, 1978). Therefore, it is rather reasonable that the second line with a slope of 1.46 is the metamorphic reaction line. According to the simple solution to equation (1) by Grant (1986), it can be obtained that F_v=0.61 counted by means of the density of rocks, i.e., there is a large amount of SiO_2 loss, alkali and some other mobile elements such as LREEs in the ductile systems, which accords to the observation of geology and experiment of geochemical data. For instance, the feldspar in the mylonite sample of the ductile shear zone is much less than in that of the wall rock (gneiss), which can be explained as the effect of ductile shearing and feldspar grain reduction (even breakdown) during mylonitization. In fact, feldspars were often replaced by muscovite and epidote in the model observation. According to the analysis and the petrologic observation, the following chemical reactions are suitable for the ductile shear zone in this region (Bryant, 1966; O'hara, 1988).

Table 7 The calculated gain and loss of different components from the ductile shear zone in the south Tan-Lu fault belt

Rock	Gneiss $\rho = 2.59$	Mylonite $\rho = 2.64$	Gain or Loss $F_v = 0.61$	Gneiss $\rho = 2.60$	Mylonite $\rho = 2.64$	Gain or Loss $F_v = 0.75$	Gneiss $\rho = 2.590$	Mylonite $\rho = 2.640$	Gain or Loss $F_v = 0.52$
SiO_2	75.04	73.46	−29.36	72.25	70.16	−18.82	72.66	69.89	−35.76
TiO_2	0.16	0.21	−0.03	0.35	0.40	−0.05	0.15	0.39	+0.06
Al_2O_3	13.26	12.95	−5.21	13.07	14.72	−1.86	1.22	1.48	−0.44
TFe_2O_3	1.00	2.10	0.25	2.80	2.90	−0.58	2.00	2.90	−0.48
CaO	1.10	1.19	−0.36	1.05	1.60	+0.17	1.22	1.48	−0.44
MgO	0.09	0.31	+0.10	0.29	0.57	+0.14	0.31	0.55	−0.02
MnO	0.01	0.03	+0.01	0.02	0.04	+0.01	0.03	0.03	−0.01
Na_2O	3.20	3.46	−1.05	3.32	4.00	−0.27	3.28	3.83	−1.26
K_2O	5.40	4.60	−2.54	5.20	3.73	−2.36	5.00	3.74	−3.03
P_2O_5	0.02	0.05	+0.01	0.03	0.01	−0.02	0.05	0.10	0.00
CO_2	0.09	0.13	−0.01	0.14	0.17	−0.01	0.34	0.25	−0.21
H_2O	0.52	0.68	−0.10	0.68	0.62	−0.21	0.76	0.70	−0.39
L.I.O	0.42	0.40	−0.17	0.67	0.52	−0.27	0.51	0.67	−0.16
Ce	46.13	50.98	−1.44	53.13	29.63	−3.06	48.21	47.67	−2.30
Pr	5.90	6.40	−0.19	6.97	6.48	−0.20	5.90	6.04	−0.27
Nd	25.56	28.22	−0.80	30.39	1.40	−2.93	26.05	27.53	−1.15
Sm	5.78	6.66	−0.16	6.69	8.91	0.01	5.87	5.7	−0.29
Eu	1.20	1.30	−0.04	1.48	1.86	−0.01	1.20	1.25	−0.05
Gd	7.42	8.19	−0.23	9.53	9.59	−0.22	8.27	8.35	−0.39
Tb	1.34	1.57	−0.04	1.90	1.90	−0.05	1.45	1.53	−0.06
Dy	8.50	9.06	−0.29	100	6.01	−0.54	9.33	9.42	−0.44
Ho	1.71	1.78	−0.06	1.98	0.68	−0.15	1.6	1.65	−0.07
Er	5.02	5.97	−0.13	6.25	4.50	−0.28	5.00	5.50	−0.21
Tm	0.59	0.67	−0.02	0.69	0.67	−0.02	0.58	0.59	−0.03
Yb	3.93	4.38	−0.12	4.59	15.29	+0.71	3.87	3.99	−0.18
Lu	0.59	0.63	−0.02	0.68	122	+9.22	0.56	0.59	−0.02
Y	8.87	14.06	−0.01	8.65	181	+12.92	8.63	12.75	−0.19
Zr	75	121	+0.02	76	51	−3.72	73	120	−0.96
Sr	158	179	−4.67	188	28	−16.67	165	176	−7.21
Pb	45	51	−1.33	54	8	−4.79	45	48	−1.97
Zn	20	25	−0.45	30	28	−0.87	22	24	−0.93
Cu	5	6	−0.13	9	27	+1.16	5	6	−0.18
Ba	1200	1334	−37.06	1480	19	−146.55	1180	1199	−54.69
Cr	24	25	−0.85	28	18	−1.43	22	23	−0.99
V	16	18	−0.48	13	26	+0.68	15	17	−0.60
Ga	18	18	−0.68	21	4	−1.80	18	18	−0.85
Nb	22	24	−0.71	26	140	+8.06	22	24	−0.93
Ni	4	4	−0.15	5	1.7	−0.37	4	4	−0.19
Rb	120	138	−3.42	159	6.2	-15.43	118	129	-4.99

Notes: Using the average components of the rocks in the same ductile shear zone, TFe_2O_3 indicates the total Fe calculated as Fe_2O_3; "+" and "−" represent the gain and loss of the element, respectively; the major elements are in g/100 g, and the trace elements in μg/100g.

$$3/2KAlSi_3O_8 \text{ (K-feldspar)} + H^+ = 1/22KAl_3Si_3O_{10}(OH) \text{ (muscovite)} + K^+ + 3SiO_2 \quad (2)$$

$$Na_4CaAl_6Si_{14}O_{40}\text{(Olioclase)} + 1.5KAlSi_3O_8\text{(K-feldspar)} + 0.5K^+ + 0.5H_2O + 3.5H^+ = 0.5Ca_2Al_3Si_3O_2(OH)\text{(Zoisite)} + 2KAl_3Si_3O_{10}(OH)\text{(Muscovite)} + 11SiO_2 + 4Na^+ \quad (3)$$

Equation (2) represents the loss of K and Si in K-feldspar by hydrolysis during mylonitization; equation (3) represents the breakdown of K-feldspar and plagioclase under ductile shearing and fluid flowing during mylonitization, which caused the increase of muscovite and epidote in the deformed tectonic rocks.

From the above discussion, it can be inferred that F_v=0.71 is reasonable in this reaction.

The C_n^A-C_n^B plots for the other chemical reaction pairs in the ductile shear zone (TL10→TL09; TL12→TL11) are also shown in Fig. 8b and c. The F_v values for each ductile shear zone are determined as 0.75 and 0.52, respectively.

According to the F_v values obtained from the diagrams and the chemical compositions in Tables 5 and 6, the gain and loss of each component can be calculated in the metamorphic reaction in the formation of ductile shear zone according to equation (1), so that the quantitative gain and loss of different chemical compositions in the ductile shear zone can be obtained. The results are listed in Table 7.

With the results of calculated gain and loss of each element, we can calculate the chemical equations for each ductile shear zone, the results of which are listed in Table 8. When counting the balance of each reaction, we only take the major elements (including Ba) in consideration, the trace elements (except Ba) do not influence the equation much (except Ba, whose gain or loss is only several to 100 μg/100 g, see Table 8), so we do not include the gain or loss of trace elements in the calculation of the chemical reactions.

5.4 Fluid/rock ratio

On the basis of the experiment results of Frourier and Potter (1982), the solubility of silica in water is

Table 8 Chemical reaction equations for the ductile shear zone, the south Tan-Lu fault belt

Reaction pair	Chemical reaction equation
TL07→TL08	100 g [sample TL07] −29.36 g SiO_2−0.03 g TiO_2−5.21g Al_2O_3−0.36 g CaO−0.29 g MgO−1.05 g Na_2O−2.54 g K_2O−0.0.04 g Ba = 61.17 g [sample TL08] +0.25 g TFe_2O_3+0.03 g P_2O_5+ 0.14 g CO_2+ 0.68 g H_2O^++0.67 g L.I.O.
TL10→TL09	100 g [sample TL10] −18.82 g SiO_2−0.05 g TiO_2−0.58 g TFe_2O_3−1.86 g Al_2O_3+0.27 g Na_2O−2.36 g K_2O−0.02 P_2O_5−0.01 g CO_2− 0.21 g H_2O^+ −0.27 L.I.O. −0.15 g Ba = 74.40 g [sample TL09] +0.17 g CaO+0.14 g MgO
TL12→TL11	100 g [sample TL12] −35.76 g SiO_2−0.44 g Al_2O_3−0.48 g TFe_2O_3−0.44 g CaO−0.02 g MgO−1.26 g Na_2O−3.032 g K_2O−0.21 g CO_2−0.39 g H_2O^+−0.16 g L.I.O. −0.05 g Ba = 57.32 g [sample TL11] +0.06 g TiO_2

Table 9 Calculated saturation of fluid/rock ratios for the ductile shear zone, the south Tan-Lu fault belt

Reaction pairs	Presumed saturation (%)				
	50	60	70	80	90
TL07→TL08	196	245	326	489	979
TL10→TL09	125	157	209	314	627
TL12→TL11	238	298	397	596	1192

approximately 3 g/kg under conditions of 300–500°C and 4 $\times 10^9$ Pa. Holland and Malinin (1979) presented 5 g/kg for the solubility of silica in water under the same conditions, which is accordant to the forming conditions of the tectonic rocks in the ductile shear zone in this study. According to the loss of the calculated SiO_2 in mylonite relative to the protolith, silica loss can be given by the following expression:

$$W_r/X_{Si}=W_f\times\delta\times(1-S) \quad (4)$$

where W_r and W_f – the total amounts of rocks and fluids respectively; X_{si} – loss of SiO_2 in the metamorphic reaction (wt %); δ – solubility of SiO_2 in the hydrothermal system (here we use the mean value 4 g/kg); S – saturation of the fluids.

Assuming that the fluids are saturated in the ductile shear zone, the fluid/rock ratios can be obtained. If the saturation is assumed to be between 50% and 90% (e.g., O'hara, 1988), the fluid/rock ratio of each ductile shear zone under different fluid saturation can be calculated (Table 9).

The calculated results for the fluid/rock ratios range from 196 to 1192, from which it can be inferred that the ductile shear zone has quite different fluid/rock ratios. It can also be inferred that the fluid in the ductile shear zone may be of a smaller scale, and the ductile shear zone may serve as a conduit for the fluid flowing.

6 Discussion

The petrology of the tectonic rocks in the ductile shear zone of the south Tan-Lu fault belt represents dynamic recrystallization of quartz, feldspar and biotite grain-size reduction and hydrolysis, thus feldspar and biotite can be changed into muscovite and zoisite. In structure, the tectonic rocks represent the orientation of tectonic movement, such as schistosity, banding, streak and augen and some minerals were strongly deformed by the effect of strong stress. However, the geochemical behaviors are hiding. The calculated results show that the volume of the mylonites relative to their protoliths is somewhat in loss, and the maximum loss can reach as high as 48% (TL12→TL11), which is correlated to the ductile shearing and fluid flowing. For example, the largest volume loss is in the metamorphic reaction of (TL12→TL11) with the largest loss of SiO_2. There are large differences of loss in the different metamorphic reaction pairs, i.e., the largest loss of SiO_2 is 35.76 g/100 g (reaction TL12→TL11) compared to the smallest loss 18.82 g/100 g (TL10→TL09). The other elements Al_2O_3, Na_2O and K_2O are lost in some percentages, whereas ΣFe_2O_3 and H_2O^+ have a little gain.

Many scholars lay emphasis on the importance of fluid interaction during ductile shearing and mylonitization. Fluids and metamorphic reactions can strongly influence the mechanical properties of rocks during their deformation in the ductile shear zone. Chemical changes clearly accompany deformation within some small-scale shear zones (e.g., Beach, 1976, 1980; Kerrich et al., 1977; Brodie, 1980, Borges and White, 1980; Sinha et al., 1986; O'hara, 1988; Miller, 1988; Kolb et al., 2000). Although Ferry (1986) studied and pointed out that the fluid/rock ratio could not be larger than 5, and some other scholars also pointed out that it was impossible for a large amount of fluids to flow in the deep crust (e.g., Valley, 1986; Wood et al., 1986). However, Beach et al. (1972), Etheridge et al. (1984), Kerrich et al. (1986), Fyfe et al. (1985), Sinha et al. (1986) and O'hara et al. (1988, 1989) revealed that there was a large amount of fluids flowing during the ductile shearing. Sinha et al. (1986) calculated the fluid/rock ratio as 250 in the Brevard ductile shear zone in the Appalachian Mountains; O'hara et al. (1988) obtained a fluid/rock ratio of more than 1000 when studying the ductile shear zones in Hot Spring Window from North California. Newman et al. (1993) got even a large amount of volume loss with 75% at Linville Fall from North California, indicating that there exists three-dimensional network of higher fluid flow through the channels along the fault zone during the mylonitization. Yang et al. (1998a) studied the fluid-assisted mass transfer processes of an upper amphibolite facies shear zone, developed in inter-layered mafic and felsic layers with geochemical evidence indicating that the chemical changes in the deformed rocks result from mixing of the mafic and felsic layers together with fluid-assisted mass transfer within the shear zone. During the

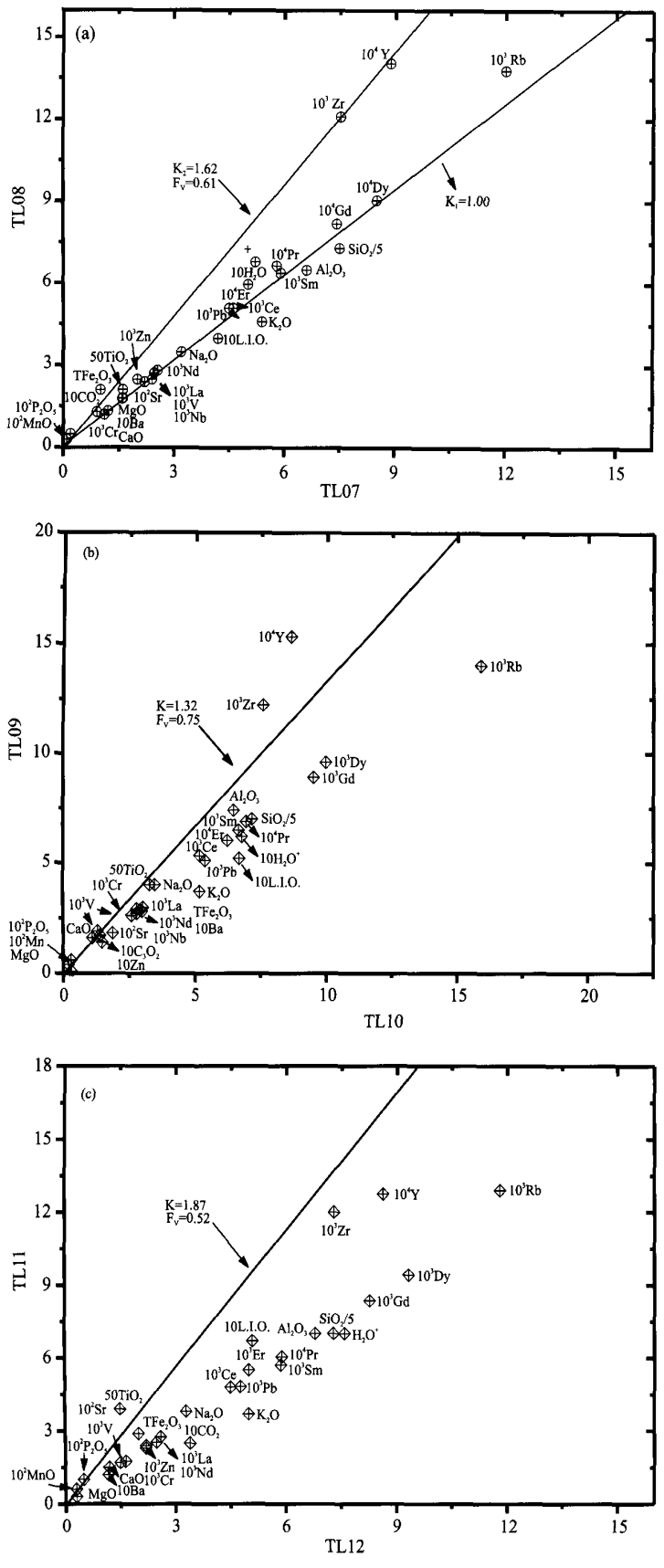

Fig. 8. Plot of composition of gneiss versus composition of its adjacent mylonites (Tables 5 and 6) on a Grant-type diagram (Grant, 1986) for each metamorphic reaction pair in the south Tan-Lu fault belt.

All the concentrations are in wt%. When drawing, the elements were scaled arbitrarily to fit on the diagram (e.g., $50TiO_2$, $SiO_2/2$ and 10^3Ce). (a) In the case, M^B/M^A =1.62, F_v=0.61; (b) M^B/M^A =1.32, F_v=0.75; (c) M^B/M^A =1.87, F_v=0.52.

mylonitization, most major elements and some trace elements (LREEs, Rb, Sr, Ba, Cu, and Ni) exhibited a mobile behavior, while the HREEs, Ti, V, Sc, Co and Fe were immobile. Our case for the element mobility seems the same with their study. The immobile element enrichments are attributed to enrichments in residual phases such as ilmentite, zircon, apatite and epidote (see Table 2 and Fig. 2) in mylonites and are interpreted as due to volume losses from 25 to 48% in different chemical reaction pairs.

Deformation changes or creates pores and fracture space and hence the permeability of rocks and, as in dissolution-precipitation creep, can drive diffusion transport along stress induced gradients in chemical potential (Wallner, 1989; Bons, 1998). Brace et al. (1966) reached a similar conclusion that the fracture of feldspar could cause dilatancy, i.e., allowing access of fluids, which is essential for the chemical reaction in equation (2) to proceed. A recent study on the influence of grain boundary fluids from the microstructure of quartz-feldspar mylonites has proved this observation (Mancktelow and Pennacchioni, 2004). There are strong similarities between low-grade vein and pressure fringe/shadow structures and high-grade migmatitic structures where melts are involved.

The recognition of structures resulting from deformation induced or enhanced material transport in or with fluids and the knowledge of their formation mechanisms give an insight in the role and activity of fluids in the crust. Bauer et al. (2000) indicated by experiments that fluid flow along deep crustal mylonitic shear zones is probably limited by the rate at which the tips of the dilatant shear surfaces propagate subparallel to the shearing plane.

The access of fluids along micro-cracks may

also promote hydrolytic weakening in quartz (Tullis et al., 1989) and feldspars and leading to further weakening (Kronenberg et al., 1987; Segall and Simpson, 1986; Tullis et al., 1996), and, together with the effect of regional stress, causing formation of the ductile shear zones, which could act as the passage way for the fluid flowing (Ramsay et al., 1973; Severstone et al., 1991). Fluids alter mineral assemblages and rates of chemical and mechanical processes during deformation, which may lead to weakening of fault-related rocks and localization of slip zones (Brantley et al., 1990; James et al., 1995). Tullis et al. (1996) proved by an experiment at 900°C and 1.4 GPa that the distribution of an aqueous fluid in fine-grained feldspar aggregates changes from isolated pores under hydrostatic conditions to mostly wetted grain boundaries during deformation, which could be used to explain the localization of strain and enhancement of bulk transport in ductile shear zones.

7 Conclusion

Mylonitization in the south Tan-Lu fault belt occurred at temperatures between 446 and 484°C on the basis of calculation of feldspars and mineral assemblages. The differential flow stress of the deformed rocks calculated from dislocations of deformed quartz ranges from 100 MPa to 210 MPa. The mylonites are enriched by factors of 1.32–1.87 in elements such as TiO_2, P_2O_5, MnO, Y, Zr and V in the ductile shear zone and depleted in SiO_2, Na_2O, K_2O and Al_2O_3 compared to their protolith gneiss. The amount of SiO_2 loss ranges from 18.82 to 35.76 g/100 g and the volume loss from 25 to 48% in different metamorphic reaction pairs within the ductile shear zone. Modeling calculated results of fluid/rock ratios for fluids flowing through the ductile shear zone range from 196 to 1192 by assuming different degrees of fluid saturation. Oxygen isotopic changes of quartz and feldspar and the calculated fluid correspond to the variations of differential flow stress in the ductile shear zone. With increasing differential flow stress, mylonites show a slight decrease of $\delta^{18}O$ in quartz, K -feldspar and fluid.

Acknowledgements

This study is supported by the National Natural Science Foundation of China (Grant 40473021), the National 973-Project of the Ministry of Science and Technology of China (2003CB214600), and the Foundation of the State Key Laboratory of Geological Processes and Mineral Resources, China University of Geosciences, and the jointed project of Max-Planck-Institute of Society and Chinese Academy of Sciences in Max-Planck-Institute of Nuclear Physics, Heidelberg, Germany. Prof. Dr. Wagner G.A. kindly revised the English and gave valuable suggestions to improve this manuscript.

Manuscript received July 25, 2006
accepted Dec 14, 2006
edited by Zhu Xiling

References

Arjan, H.D., Martyn, R.D., Reinoud, L.M.V., and Julie, N., 2002. On the role of melt-rock reaction in mantle shear zone formation in the Othris Peridotite Massif (Greece). *J. Struct. Geol.*, 24: 1431–1450.

Bauer P., Palm S., and Handy M.R., 2000. Strain localization and fluid pathways in mylonite, inferences from in situ deformation of a water-bearing quartz analogue (norcamphor). *Tectonophysics*, 320, 141–165.

Beach, A., 1976. The interrelations of fluid transport, deformation, and geochemistry and heat flow in early Protrusion shear zones in the Lewis Ian complex. *Phil. Trans. Roy. Soc. Lond.*, A280: 690–-604.

Beach, A., 1980. Retrogressive metamorphic processes in shear zones with special reference to the Lewis Ian complex. *J. Struct. Geol.*, 2: 257–263.

Beach, A., and Fyfe, W.S., 1972. Fluid transport and shear zones at Sourie, Switzerland: Evidence of overthrusting. *Contrib. Mineral. Petrol.*, 36: 175–179.

Bons, P.D., 1998. Apparent extensional structures due to volume loss. *Proc. Estonian Acad. Sci. Geol.*, 48: 3–14.

Borges, F. S., and White, S. H., 1980. Microstructural and chemical studies of sheared anorthosites, Roneval, South Harris. *J. Struct. Geol.*, 2: 273–280.

Brace, W.F., Paulding, B.W., and Scholtz, C., 1966. Dilatancy in the fracture of crystalline rocks. *J. Geophy. Res.*, 71: 3939–3953.

Brantley, S.L., Evans, B., Hickman, S.H., and Crera, D.A., 1990. Heating of microcracks in quartz: Implications for fluids flow. *Geology*, 18, 136–139.

Brodie, K.H., 1980. Variations of mineral chemistry across a shear zone in phlogophite peidotite. *J. Struct. Geol.*, 2: 265–272.

Bryant, B., 1966. Formation of phyllinites in the Grandfather Mountain area, northwestern North Carolina. *US Geol. Surv. Prof. Pap*, 550-D: 144–150.

Burkhard, M., and Kerrig, R., 1988. Fluid regimes in the deformation of Helvetic nappes, Switzerland, as inferred from stable isotope data. *Contrib. Mineral. Petrol.*, 99: 416–429.

Cann, J.R., 1970. Rb, Sr, Y, Zr and Nb in some ocean floor basaltic rocks. *Earth Planet. Sci. Lett.*, 10: 7–11.

Clayton, R.N., O'Neil, J.R., and Meyeda, T.K., 1972. Oxygen isotope exchange between quartz and water. *J. Geophy. Res.*, 77: 3057–3067.

Correns, C.N., 1978. Titanium, behavior in metamorphic reactions. In: Wedeppohl, K.H. (ed.), *Handbook of Geochemistry*, 2(IV), Berlin: Springer, 67.

Christinie, J.M., and Ord, A., 1980. Flow stress from microstructures of mylonites: Example and current assessment. *J. Geophy. Res.*, 85: 6253–6262.

Dong Shuwen, Zheng Yadong, Chen Xuanhua and Shi Jing, 2006. Advances in structural geology and tectonics in the late 20th Century: A review. *Acta Geologica Sinica* (English edition), 80 (3): 349–375.

Etheridge, M.A., and Wilkie, J.C., 1981. An assessment of dynamically recrystallized grain size as a paleopiezometer in quartz-bearing mylonite zone. *Tectonophysics*, 78: 475–508.

Etheridge, M.A., Wall, V.J., and Cox, S.F., 1984. High fluid pressures during regional metamorphism and deformation: Implications for mass transport and deformation mechanism. *J. Geophy. Res.*, 89: 4344–4358.

Faure, G., 1978. Strontium, behavior during weathering and rock alteration. In: Wedeppohl, K.H. (ed.), *Handbook of Geochemistry*, 2(IV). Berlin: Springer, 67.

Ferry, J. M., 1986. Infiltration of aqueous fluid and high fluid rock ratios during green schist facies metamorphism: A reply. *Journal of Petrology*, 27: 695-712.

Fournier, R.O., and Potter, R.W., 1982. An equation correlating the solubility of quartz in water from 25°C to 900°C at pressures up to 10,000 bars. *Geochem. Cosmochem. Acta*, 46: 1969–1973.

Fountain, D.M., Boundy, T.M., Austrheim, H., and Rey, P., 1994. Eclogite-facies shear zones — deep crustal reflectors. *Tectonophysics*, 232: 411–424.

Fyfe, W.S., and Kerrich, R., 1985. Fluid and thrusting. *Chem. Geol.*, 47: 353–362.

Gibson, R.G., 1990. Nucleation and growth of retrograde shear zones, an example from the Needle Mountains, Colorado, U.S.A. *J. Struct. Geol.*, 12: 339–350.

Glazner, A.F., and Barttey, J.M., 1991. Volume loss, fluid flows and state of strain in extension mylonites from the central Mojave Desert, California. *J. Struct. Geol.*, 13: 587–594.

Gresens, R.L., 1967. Composition-volume relationships of metasoamatism. *Chem. Geol.* 2: 47–65.

Grant, J.A., 1986. The isocorn diagram — a simple solution to Greasens equation for metasomatic alteration. *Econom. Geol.*, 81: 1976–1982.

Hacker, B.R., An, Y., Christie, J.M., and Davis, G.A., 1992. Stress magnitude, strain rate, and rheology of extended middle continental crust inferred from quartz grain size in Whipple Mountains, California. *Tectonics*, 11: 36–46.

Herrmann, A.G., 1978. Yttrium, Abundance in natural waters. In: Wedeppohl, K.H. (ed.), *Handbook of Geochemistry*, 2(IV), Berlin: Springer, 57.

Holland, H.D., and Malinin, S.D., 1979. The solubility of non-ore minerals. In: Barnes, H.L. (ed.), *Geochemistry of Hydrothermal Ore Deposits* (2nd ed.), New York: Wiley, 798.

Hou Zengqian, Yang Zhusen, Li Yinqing, Zeng Pusheng and Meng Yifeng, 2004. Large-scale migration of fluids toward foreland basins during collisional orogeny: Evidence from Triassic anhydrock sequences and regional alteration in the middle-lower Yangtze area. *Acta Geologica Sinica* (English edition), 78(1): 203–220.

James, V.G., and James, P.E., 1995. Chemical changes and fluid-rock interaction in faults of crystalline thrust sheets, northwestern Wyoming, U.S.A. *J. Struct. Geol.*, 17: 533–547.

Jefferies, S.P., Holdsworth, R.E., Wibberley, C.A.J., Shimamoto, T., Spiers, C.J., Niemeijer, A.R., and Lloyd, G.E., 2006. The nature and importance of phyllonite development in crustal-scale fault cores: An example from the Median Tectonic Line, Japan. *J. Struct. Geol.*, 28: 220–235.

Julie, N., William, M.L., Martyn, R.D., and Reinoud, L.M.V., 1999. Deformation processes in a peridotite shear zone: Reaction-softening by an H_2O-deficient, continuous net transfer reaction. *Tectonophysics*, 303: 193– 222.

Kisters, A.F.M., Kolb, J., Meyer, F.M., and Hoernes, S., 2000. Hydrologic segmentation of high-temperature shear zones: Structural, geochemical and isotopic evidence from auriferous mylonites of the Renco mine, Zimbabwe. *J. Struct. Geol.*, 22: 811–829.

Kerrich, R., Fyfe, W.S., Corman, B.E., and Allison, I., 1977. Local modification of rock chemistry by deformation. *Contrib. Mineral. Petrol.*, 65: 183–190.

Kerrich R., 1986. Fluid infiltration into the fault zones, chemical, isotopic and mechanical effects. *Pure Applied Geophysics*, 124: 225–268.

Kolb, J., Kisters A.F.M., Hoernes, S., and Meyer, F.M., 2000. The origin of fluids and nature of fluid-rock interaction in mid-crustal auriferous mylonites of the Renco mine, southern Zimbabwe. *Mineralium Deposita*, 35: 109–125.

Kronenberg, A.K., Segall, P., and Wolf, G.H., 1990. Hydrolytic weakening and penetrative deformation within a natural shear zone. *American Geophysical Union Monograph Series*, 56: 21 –36.

Landergren, S., 1978. Vanadium, Solubility of compounds which control concentrations of vanadium in natural water, In: Wedeppohl, K.H. (ed.), *Handbook of Geochemistry*, 2(IV), Berlin: Springer, 23.

Lin, A., Miyata, T., and Wan, T. 1998. Tectonic characteristics of the central segment of the Tancheng-Lujiang fault zone, Shandong Peninsula, eastern China. *Tectonophysics*, 293 (1 – 2): 85 – 104.

Lin, W., Faure, M., Wang, Q.C., Monie, P., and Panis, D., 2005. Triassic polyphase deformation in Feidong-Zhangbaling massif (eastern China) and its place in collision between the North China and South China blocks. *J. Asian Earth Sci.*, 25: 121 – 136.

Lu, H.F., Yu, H.N., Ding, Y.W., and Zhang Q.L., 1983. Changing stress field in the middle segment of the Tan-Lu fault zone, eastern China. *Tectonophysics*, 98: 253–270.

Mancktelow, N.S., and Pennacchioni, G., 2004. The influence of grain boundary fluids on the microstructure of quartz-feldspar mylonites. *J. Struct. Geol.*, 26: 47–69.

Mattauer, M., Matte, Ph., Malavielle, J., Tapponnier, P., Maluski, H., Xu Zhiqin, Liu Yilun and Tang Yaoqin, 1985. Tectonics of the Qinling belt: Build-up and evolution of eastern Asia. *Nature*, 317: 496–500.

Mattey, D., Jackson, D.H., and Harris, N.B., 1994. Isotopic constrains on fluid infiltration from an ecologite facies shear zone, Holsendy, Norway. *J. Metamor. Geol.*, 12: 311–331.

McCaig, A.M., 1988. Deep fluid circulation in fault zones. *Geology*, 16: 867–870.

Mercier, J.-C.C., Anderson, D.A., and Carter, N.L., 1977. Stress in the lithosphere, inferences from steady state flow of rocks. *Pure Applied Geophysics*, 115: 199–266.

Mulch, A., Cosca, M.A. and Handy, M.R., 2002. In-situ UA-laser $^{40}Ar/^{39}Ar$ geochronology of a micaceous mylonite: An example of defected-enhanced argon loss. *Contrib. Mineral. Petrol.*, 142: 738–752.

Miller, R.B., 1988. Fluid flow, metamorphism and amphibole deformation in an imbricated ophiolite, North Cascades, Washington. *J. Struct. Geol.*, 10: 283–296.

Müller, R.F., and Saxena, S.K., 1977. *Chemical Petrology*. Heidelberg: Springer-Verlag, 394.

Müller, W., Mancktelow, N.S., and Meier, M., 2000. Rb-Sr microchrons of synkinematic mica in mylonites: An example from the DAV fault of the Eastern Alps. *Earth Planet. Sci. Lett.*, 180: 385–397.

Newman, J., and Mitra, G., 1993. Lateral variations in mylonite zone thickness as influenced by fluid-rock interactions, Linvill Falls fault, North Carolina. *J. Struct. Geol.*, 15: 849–863.

O'hara, K.D., 1988. Fluid flow and volume loss during

mylonitization, an origin for phyllonite in an overthrust setting, North California. *Tectonophysics,* 156: 21–36.

O'hara, K.D., 1994. Fluid-rock interaction in crustal shear zones, a directed dislocation approach. *Geology*, 22: 843–846.

O' hara, K.D., and William, H.B., 1989. Volume-loss model for trace-element enrichments in mylonites. *Geology*, 19: 893–896.

O'Neil, J.R., and Taylor, H. Jr., 1967. The oxygen isotope and cation exchange chemistry of feldspars. *American Mineralogist*, 52: 1414–1437.

Paterson, S., and Vernon, K., 1995. Bursting the bubble of ballooning plutons: A return to nested diapers emplacement by multiple processes. *Geol. Soc. Am. Bull.*, 107: 1356–1380.

Pennacchioni, G., 1996. Progressive eclogitization under fluid-present conditions of pre-Alpine mafic granulites in the Austroalpine Mt Emilius Klippe (Italian Western Alps). *J. Struct. Geol.,* 18: 549–561.

Pennacchioni, G., and Cesare, B., 1997. Ductile-brittle transition in pre-Alpine amphibolite facies mylonites during evolution from water-present to water-deficient conditions (Mont Mary nappe, Italian Western Alps). *J. Metamor. Geol.*, 15: 777–791.

Phillips, R.J., Parrish, R.R., and Searl, M. P., 2004. Age constraints on ductile deformation and long-term slip rates along the Karakoram fault zone, Ladakh. *Earth Planet. Sci. Lett.,* 226: 305–319.

Ramsay, J.G., and Wood, D.S., 1973. The geometric effects of volume change during deformation process. *Tectonophysics*, 16: 263–277.

Samantaa, S.K., Mandala, N., and Chakraborty, C., 2002. Development of different types of pull-apart microstructures in mylonites: An experimental investigation. *J. Struct. Geol.,* 24: 1345–1355.

Schenk, O., Urai, J.L., and Evans, B., 2005. The effect of water on recrystallization behavior and grain boundary morphology in calcite — observations of natural marble mylonites. *J. Struct. Geol.,* 27: 1856–1872.

Severstone, J., Morteani, G., and Staude, J.M., 1991. Fluid channeling during ductile shearing transformation of granodiorite into aluminous schist in the Tauern window (East Alps). *J. Metamorphic Geol.*, 9: 419–431.

Segall, P., and Simpson, C., 1986. Nucleation of ductile shear zones on dilatants fractures. *Geology*, 14: 56–59.

Sinha, K.A., Hawwit, D.A., and Rimstidt, J.D., 1986. Fluid interaction and element mobility in the development of ultramylonites. *Geology*, 14: 883–886.

Streit, J.E., and Cox, S.F., 1998. Fluid infiltration and volume change during mid-crustal mylonitization of Proterozoic granite, King Island, Tasamania. *J. Metamor. Geol.*, 16: 197–212.

Tobisch, O.T., Barton, M.D., Vermon, R.H., and Paterson, S.R., 1991. Fluid-induced deformation, transformation of granitoids to banded mylonites, western Sierra Nevada, California, and southeastern Australia. *J. Struct. Geol.,* 13: 1137–1156.

Torgeir, R.F., Andersen, B., and Wheeler, J., 2005. Eclogite-facies polyphase deformation of the Drøsdal eclogite, Western Gneiss Complex, Norway, and implications for exhumation. *Tectonophysics*, 398: 1–32.

Tullis, J., Snoke, A.W., and Todd, V.R., 1982. Significance and petrogenesis of mylonite records. *Geology*, 10: 227–230.

Tullis, J., Yund, R., and Faver, J., 1996. Deformation-enhanced fluid distribution in feldspar aggregates and implications for ductile shear zones. *Geology*, 24: 63–66.

Twiss, R.J., 1977. Theory and applicability of recrystallized grain size paleopiezometer. *Pure Applied Geophysics,* 5: 337.

Twiss, R.J., 1986. Variable sensitivity piezometric equations for dislocation density and subgrain diameter and their relevance to olivine and quartz. *American Geophysical Union (Geophysical Monograph)*, 36: 247–261.

Valley, J.W., 1986. Stable isotope geochemistry of metamorphic rocks. In: Ribbe, P.H. (ed.), *Stable Isotopes. Review in Mineralogy,* Mineralogical Society of American, 16: 445–481.

Wallner, H., 1989. Porous rock deformation and fluid flow — numerical FE-simulation of the coupled system. *Geologische Rundschau*, 78: 171–182.

Wang Zhihong and Lu Huafu, 2000. Ductile deformation and $^{40}Ar/^{39}Ar$ dating of the Changle-Nanao ductile shear zone, southeastern China. *J. Struct. Geol.,* 22: 561–570.

Wenk, H.-R., 1994. Preferred orientation patterns in deformed quartzites. *Review in Mineralogy*, 29: 176–208.

Whitney, J.A., and Stomer, J.R., 1977. The distribution of $NaAlSi_3O_8$ between coexisting microcline and plagioclase and its effect on geothermometric calculations. *Am. Mineral.*, 62: 687–691.

Wood, B.J., and Walther, J.V., 1986. Fluid flow during metamorphism and its implications for fluid-rock ratios. In: Walther, J.V., and Wood, B.J. (eds.), Fluid-rock Interactions during metamorphism. *Advances in Physical Geochemistry*, Berlin: Springer, 5: 89–108.

Xu, J.W., Zhu, G., Tong, W.X, Cui, K.R., and Liu, Q., 1987. Formation and evolution of the Tancheng-Lujiang wrench fault system, a major shear system to the northwest of the Pacific Ocean. *Tectonophysics*, 134: 273–310.

Yang, X.Y., O'hara, K.D., and Moecher, D.P., 1998a. Distinction between tectonic mixing and mass transfer processes in a ductile shear zone. *J. Struct. Geol.,* 20: 1089–1103.

Yang Xiaoyong, Yang Xueming, Liu Deliang, Wang Kuiren and Dai Jinxing, 1998b. Micro-structural evidences of tectonic superimposition (compound) by south part of Tancheng-Lujiang fault and Dabie-Jiangnan orogenic belt, China. *Acta Geophysica Sinica*, 41(Sup.): 123–132 (in Chinese with English abstract).

Yang X.Y., Liu, D., and Wagner, G.A., 2001. Conditions of deformation and variations of compositional and structural state of feldspars during mylonitizaton: Exemplified from the ductile shear zones in south Tan-Lu fault belt of China. *Neues Jahrbuch für Mineralogie (Mon.)*, H(9–10): 415–432.

Zhang Jiasheng, 1992. The Characteristics and significance of Tan-Lu fault belt. *J. China Univ. Geosci.*, 18: 363–371 (in Chinese with English abstract).

Zhu Guang, Hou Minjin, Wang Yongsheng, Liu Guosheng and Niu Manlan, 2004. Thermal evolution of the Tanlu fault zone on the eastern margin of the Dabie Mountains and its tectonic implications. *Acta Geologica Sinica* (English edition), 78(4): 940–953.